Check for updates

Investigation on the physical properties and biocompatibility of zirconia–alumina-silicate@diopside composite materials and its *in vivo* toxicity study in embryonic zebrafish†

Tanawut Rittidach,[a] Siwapech Sillapaprayoon,[b] Varissara Chantho,[b] Wittaya Pimtong,[b] Narattaphol Charoenphandhu,[cdef] Jirawan Thongbunchoo,[cd] Nateetip Krishnamra,[cd] Atipong Bootchanont, [g] Porramain Porjai[g] and Weeraphat Pon-On *[a]

Bioceramic materials have a wide range of applications in the biomedical field, such as in the repair of bone defects and dental surgery. Silicate-based bioceramics have attracted biomedical researchers' interest due to their bioactivity and biodegradability. In this study, extended the scope of ZAS utilization in bone tissue engineering by introducing calcium–magnesium-silicate (diopside, CMS) as an interface material aim to develop a machinable bioceramic composite (ZASCMS) by the sol–gel method. The physicochemical characterization, *in vitro* biological properties and *in vivo* zebrafish cytotoxicity study of ZAS-based composites as a function of CMS contents, 0, 25, 50, 75 and 100 wt%, were performed. Results showed that the as-prepared ZASCMS possessed porous architecture with well-interconnected pore structure. Results also revealed that the mechanical properties of ZASCMS composite materials were gradually improved with increasing CMS contents. The ZASCMS composites with more than 50 wt% CMS had the highest compressive strength and modulus of 6.78 ± 0.62 MPa and 340.10 ± 16.81 MPa, respectively. Regarding *in vitro* bioactivities, the composite scaffolds were found to stimulate osteoblast-like UMR-106 cell adhesion, growth, and proliferation. The antibacterial activity of the ZASCMS composite scaffolds was tested against *Staphylococcus epidermidis* (*S. epidermidis*) and *Escherichia coli* (*E. coli*) also exhibited an antibacterial property. Furthermore, the *in vivo* studies using embryonic zebrafish were exposed to as-prepared particles ($0–500$ µg mL^{-1}) and showed that the synthesized ZAS, CMS and ZASCMS composite particles were non-toxic based on the evaluation of survivability, hatching rate and embryonic morphology. In conclusions, our results indicated that the synthesized composite exhibited their biological properties and antibacterial activity, which could well be a promising material with high potential to be applied in orthopaedic and dental tissue engineering.

aDepartment of Physics, Faculty of Science, Kasetsart University, Bangkok 10900, Thailand. E-mail: fsciwpp@ku.ac.th

bNano Environmental and Health Safety Research Team, National Nanotechnology Center (NANOTEC), National Science and Technology Development Agency (NSTDA), Pathum Thani 12120, Thailand

cCenter of Calcium and Bone Research, Faculty of Science, Mahidol University, Bangkok 10400, Thailand

dDepartment of Physiology, Faculty of Science, Mahidol University, Bangkok 10400, Thailand

eInstitute of Molecular Biosciences, Mahidol University, Nakhon Pathom 73170, Thailand

fThe Academy of Science, The Royal Society of Thailand, Dusit, Bangkok 10300, Thailand

gDivision of Physics, Faculty of Science and Technology, Rajamangala University of Technology Thanyaburi, Pathum Thani 12120, Thailand

† Electronic supplementary information (ESI) available. See DOI: https://doi.org/10.1039/d3ra04555b

1. Introduction

Biocomposite materials are attracting increasing attention especially in bone tissue engineering. In recent years, calcium phosphate based on hydroxyapatite (HAp), tricalcium phosphate (TCP) or biphasic mixtures of those two have become the bioceramics widely used in the production of scaffolds for treatment of bone tissue damage due to their having positive effect on osteogenesis *in vitro* and *in vivo* as well as their excellent biocompatibility.[1–5] Apart from the calcium phosphate-based biomaterials, silicate-based bioceramics have also received much attentions from bone tissue engineers because of their stimulatory effects on bone cell proliferation, differentiation and osteogenic gene expression.[6–11] Moreover, the presence of Mg demonstrated that improves the mechanical property and the degradation rate of silicate-based bioceramics, which are fundamental scaffold design concerns for bone

regeneration.[8] Some members of this silicate material species of Mg-containing Ca-silicate bioceramics are diopside ($CaMgSi_2O_6$), akermanite ($Ca_2MgSi_2O_7$) and bredigite ($Ca_7MgSi_4O_{16}$).[8–11] Each type has unique properties, for instance, diopside is bioactive and very stable *in vivo*,[8] whereas akermanite and bredigite exhibit superior osteogenic properties due to their appreciable biodegradation.[9–11] Typically, Ca–Mg-silicate of diopside is an ideal choice as a load-bearing material for bone implant. However, it does not fulfil all criteria of bone-like material and is not yet an ideal material to be use for bone repair. Thus, incorporating other appropriate materials could turn it into a more suitable bone implant material. Considering diopside (*i.e.*, $CaMgSi_2O_6$; CMS), several studies have shown that incorporating certain ions or other bioceramic materials significantly improved both physical and biological properties.[12–15] Pang *et al.*, prepared strontium and copper doped diopside, which showed mechanical improvement, superior bioactivity and strong osteogenic effect on bone cells.[12] Shen *et al.*, fabricated a core–shell structure wollastonite@-diopside scaffolds that were presented with both mechanical and biodegradable properties.[13] Ros-Tarraga and coworkers prepared diopside–wollastonite eutectic ceramics. They found that ceramic of eutectic composition performed *in vitro* experiments with adult human mesenchymal stem cells (Ah-MSCs) provided good surface for cell adhesion as well as induced high proliferation rate and an increase in the bioactivity.[14]

Herein, a composite of diopside ($CaMgSi_2O_6$, CMS) with other silicate-based bioceramic of zirconia–alumina-silicate ($2ZrO_2 \cdot [3Al_2O_3 \cdot 2SiO_2]$; zirconia–mullite) (ZAS) was synthesized by the sol–gel casting method. This composite was supposed to combine the favourable properties of individual materials used. Zirconium dioxide (zirconia) is one of the most ideal bioceramic materials because of its high mechanical properties, biocompatibility with neither inflammatory effect nor toxicity to the surrounding tissues.[15–17,20] Moreover, zirconia is available in various forms, *e.g.*, zirconia–alumina-silicate-based bioactive scaffolds, that have already been successfully synthesized and used in bone tissue engineering (BTE) applications.[15–20] Meanwhile, Ca–Mg-silicate, another alternative bioceramic material of calcium phosphate (CaP) ceramics, was selected based on its unique physicochemical such as its superior compressive strength, mechanical stability, excellent biocompatibility and osteoconductivity and its ionic extract solution being able to stimulate bone-related cell. The use of Ca–Mg-silicate-based materials prompted a new treatment for the remineralization and regeneration of bone and tooth.[21–24] In addition, the presence of bioactive elements (*e.g.*, Mg and Si) has a stimulatory effect on bone regeneration. Among the ions capable of doping, Mg is selected as the added trace element because it is an essential element in the human body, mostly found in bone and teeth, and it plays an important role in biomineralization.[25] The Mg-based biomaterial has higher hardness and inhibits bacterial growth compared to Mg-undoped materials.[26–28] Regarding Si, it has been shown to stimulate proliferation and differentiation of osteoblast-like cells.[29,30]

From our previous investigation, the synthesized ZAS combined with biphasic calcium phosphate (BCP) and a biopolymer matrix succeeded as a candidate in bone tissue engineering.[19] This present study extended the scope of ZAS utilization in bone tissue engineering by introducing calcium–magnesium-silicate (diopside, CMS) as an interface material aim to develop a machinable bioceramic composite by the sol–gel method. The synthesized composite materials were investigated on physicochemical properties, an antibacterial capacity and biocompatibility *in vitro* and *in vivo* in zebrafish model. The investigation of the biocompatibility of potential available bioceramics material is a major challenge in bone tissue engineering. Zebrafish (*Danio rerio*) provides a number of powerful advantages as a model of study due to its rapid external embryonic development. Furthermore, zebrafish share a high of genetic homology, physiological and functional conservation similar to human genetic.[45,46] From these features, recently zebrafish is very popular model to use in the fields of *in vivo* toxicology. Therefore, different concentration ratios of ZAS and CMS ($1:0, 3:1, 1:1, 1:3, 0:1$ by weight ratio) were investigated for the morphology of sample surface, mechanical properties, cell morphology, cell attachment, cell proliferation in the rat osteoblast-like UMR-106 cells, as well as their antimicrobial activity. Regarding the *in vivo* studies, particles at concentration at a dose of up to 500 µg mL^{-1} and zebrafish embryo survival, hatching and malformation rates were investigated.

2. Materials and methods

2.1 Chemical agents

Zirconium oxide (ZrO_2, Fluka Chemical, Switzerland). Aluminium chloride hydrate ($AlCl_3 \cdot 6H_2O$, Kemaus, N.S.W., Australia) and calcium chloride ($CaCl_2$, Ajax Finechem, Australia), calcium nitrate [$Ca(NO_3)_2 \cdot 4H_2O$, Kemaus, N.S.W., Australia], magnesium chloride ($MgCl_2$, Kemaus, N.S.W., Australia), tetraethyl orthosilicate (TEOS; Sigma, USA) and polyethylene glycol (Sigma, USA), hydrochloric acid (HCl; Merck, Germany), citric acid (Merck, Germany).

2.2 Preparation of zirconia–mullite ($2ZrO_2 \cdot [3Al_2O_3 \cdot 2SiO_2]$ (ZAS)) and calcium–magnesium silicate ($CaMgSi_2O_6$, CMS) (ZASCMS) composite powders

The ZAS powders were prepared by the sol–gel method as described in the previous study.[7] The ZAS powder with the chemical formula of $2ZrO_2 \cdot [3Al_2O_3 \cdot 2SiO_2]$, was obtained by uniformly mixing the 2.46 g of ZrO_2, 7.24 g of $AlCl_3 \cdot 6H_2O$, 4.17 g of TEOS, 1.5 g of 0.5 M HCl, 3 g of citric acid and 2 g of polyethylene glycol in 60 g of ethanol under constant stirring at room temperature for 2 days. Subsequently, the solution was heated at 80 °C for 4 h, during which most of the liquid portion was evaporated until a gel had formed. Then, the dried powder was sintered in electric furnace at 1200 °C for 3 h in air and then it was cooled to room temperature to afford the desired ZAS product.

Synthesis of calcium–magnesium-silicate (diopside, CMS) powders in this study was prepared by sol–gel method as described in the previous report.[7] In a typical synthesis, 1.5 g of 0.5 M HCl, 3 g of citric acid and 2 g of polyethylene glycol were

dissolved in 60 g of ethanol. After complete dissolution, 2.36 g of Ca(NO$_3$)$_2$·4H$_2$O, 2.03 g of MgCl$_2$, 4.17 g of TEOS were added in the solution. The mixture was stirred at room temperature for 2 days to form clear solution. Afterward, the solution was heated at 80 °C to form powder. The as-prepared powder was transferred in a furnace of 1200 °C for 3 h to produce the CMS powders.

The ZASCMS composite powder was obtained by direct mixing ZAS and CMS with difference mass ratios of 1 : 0, 3 : 1, 1 : 1, 1 : 3 and 0 : 1, and the products were presented as ZAS, ZASCMS25, ZASCMS50, ZASCMS75 and CMS, respectively. Briefly, different stoichiometric amounts of ZAS and CMS powders were added into the mixed solution of 5 wt% of CaCl$_2$ and 0.25 wt% of citric acid dissolved in ethanol/deionized water (4 : 1 v/v) and stirring at room temperature for 3 h to form homogeneous slurry. Afterward, the mixture was heated at 80 °C to evaporate the liquid to obtain the dry ZASCMS composite powder. The powder was calcined in an electric furnace at 900 °C for 3 h under air atmosphere to obtain the zirconia–alumina-silicate composite with diopside powders.

3. Characterization of the composite scaffolds

3.1 Physico-chemical characterization

The composition of synthesized ZAS, CMS and ZASCMS composites was confirmed by Fourier transform infrared spectroscopy (FT-IR, Spectrum GX, PerkinElmer, USA) analyses of the raw powders and was carried out on a Spectrum GX, PerkinElmer. The FT-IR spectrum was collected from the range 370–4000 cm^{-1} to determine the functionality of the composite powders. All samples were mixed with KBr and pressed into pellets and placed directly on the spectrometer.

The morphology of the as-prepared ZAS, CMS and its composites was observed by scanning electron microscopy (SEM) (JEOL model JSM-6301F, Tokyo, Japan). Meanwhile, the chemical composition of the material was determined by energy dispersion spectroscopy (EDS). All samples were coated with gold using JEOL model JSM-6301F. SEM and EDS images of the surface of the composite scaffolds and elements of scaffold surfaces were taken under an accelerating voltage of 5 kV.

X-ray diffractometer (XRD) (D8 Advance, Bruker, Germany) is widely used technique for investigation of phase composition and crystalline structure. This technique was used to study the crystal structure properties, determination of crystalline phases, *etc.* The phase composition of the composites was investigated using XRD with a CuKα radiation ($\lambda = 0.15405$ nm) in a 2θ range from 20° to 60°.

3.2 Mechanical properties

Universal testing machine (UTM, Instron model 55R4502, Instron Corp., Norwood, MA, USA) was used to measure compressive stress of dried composite cylindrical scaffolds with 10 mm diameter and 15 mm height at 5 mm min^{-1}. The modulus of elasticity was defined as $E = \sigma(t)/\varepsilon_{offset}$, where $\sigma(t)$ is stress and ε_{offset} is strain and determined as linear slope of stress–strain curve. Each test was repeated three times for each sample and the results were expressed as the average value ± standard deviation.

3.3 *In vitro* study (cell proliferation)

For the biological test, the rat osteoblast-like UMR-106 cells [American Type Culture Collection (ATCC) no. CRL-1661] were grown in a Dulbecco's modified Eagle's medium (DMEM, Sigma, USA) supplemented with 10% v/v fetal bovine serum (FBS, Austria) and 100 U per mL penicillin–streptomycin (Gibco, USA), and were seeded on the circular glass (control) and ZASCMS discs at 1×10^6 cells per well in 6 well plates, where a circular glass (1.3 cm diameter) had been placed inside. The well plates were incubated in humidified atmosphere containing 5% CO$_2$ at 37 °C. Cell attachment and mineralization were determined on day 3 after seeding. In some studies, the glass and ZASCMS composite scaffolds were briefly rinsed twice with phosphate buffer (pH 7.2) and then fixed in 2.5% glutaraldehyde (Electron Microscopy Science, Fort Washington, PA, USA) in 0.1 M phosphate buffer for 3 h. Thereafter, the glass and ZASCMS composite scaffolds were dehydrated in a graded series of ethanol solution (50%, 70%, 80%, 90% and 100% v/v ethanol) before being desiccated under vacuum. Cell morphology, adhesion and proliferation were examined by using scanning electron microscopy (SEM).

3.4 Antimicrobial test

To observe the antibacterial effect of ZAS, CMS and ZASCMS scaffolds using the agar disc-diffusion technique, two types of bacteria were used to evaluate the antibacterial activity of the material – *Staphylococcus epidermidis* (ATCC 12228), representing Gram-positive bacteria, and *Escherichia coli* (ATCC 25922), representing Gram-negative bacteria. Both bacteria were capable of causing infection at the implant site. The bacteria cultures (1 mL) were diluted in 50 mL of medium to an optical density (OD) of 600 nm and 0.5 mL of each was separately spread on LB solid medium. Both bacteria samples were cultured in a Petri dish overnight at 37 °C. The 6 mm filter papers were soaked in 20 μL water for negative control and immersed in a 20 μL of 0.1 mg mL^{-1} ampicillin solution for the positive control. The OD was determined after an overnight incubation.

To quantify ZAS, CMS and ZASCMS composite scaffolds bacterial growth on the percentage of bacterial reduction (% reduction) was measured according to ASTM E2149-13a,[31] for *Escherichia coli* (ATCC 25922) and *Staphylococcus aureus* (ATCC 6538p). The cylindrical samples with 6 mm diameter and thickness of 2 mm were incubated for 24 h (contact time) at 35 ± 2 °C with strong agitation (180 rpm). Cultures without any composite material and CMC without linked ZASCMS were used as controls. Three independent experiments were performed for this analysis. The 10^7 CFU mL^{-1} of growth control was estimated at time zero and after the contact time (t_1) to ensure that the bacterial load did not change during the contact time. The percentage of bacterial reduction was calculated for each assessment using the following eqn (1):

$$\% \text{ reduction} = \frac{B - A}{B} \times 100 \qquad (1)$$

where A is CFU mL^{-1} of the treated sample (ZAS, CMS and ZASCMS composite materials) and B is CFU mL^{-1} of the growth control or "only inoculum".

3.5 *In vivo* toxicity study of ZASCMS composite particles

3.5.1 Zebrafish maintenance and embryo collection. Adult zebrafish (*Danio rerio*) were maintained and raised at the National Nanotechnology Center (NANOTEC) in a stand-alone recirculation system (AAB-074, Yakos65, Taiwan) following standard protocols. The fish were raised under a photoperiod of 14/10 h (day/night) at 28 ± 1 °C. Embryos were obtained from natural pair-wise mating and kept in egg water (0.006% w/v sea salt in deionized water). Fertilized embryos at 4 hours post-fertilization (hpf) were selected under a stereomicroscope (SZX16, Olympus, Tokyo, Japan). All *in vivo* procedures have been approved by the NSTDA Institutional Animal Care and Use Committee.

3.5.2 Zebrafish embryo acute toxicity test. The zebrafish embryo acute toxicity test followed the Organization for Economic Co-operation and Development guideline number 236 (OECD 236, 2013).[32] Stock solutions of particles, *i.e.*, ZAS, CMS, and ZAS : CMS (1 : 1) (ZASCMS50), were prepared in deionized water and sonicated for 10 min. For test solutions, stock solutions of 1 mg mL^{-1} of each material was diluted twice (x/2), following which they were preserved different concentrations of particles in egg water to final concentrations of 31.25, 62.5, 125, 250, and 500 μg mL^{-1} and sonicated for 10 min. Twenty zebrafish embryos were exposed to 2 mL of each test solution in a 12-well culture plate with 2 mL of egg water being used as a negative control. Each test solution was vortexed for 20 s before immediate adding to the well. The plates were incubated at 28.5 ± 1 °C up to 96 h. Every 24 h the test solutions were renewed and dead embryos were removed. The survival, hatching, and malformation rates of zebrafish were recorded. Experiments with less than 90% survival in the control group were repudiated. At 24 and 48 hpf, the heart rates of embryos were recorded by using stereomicroscopic video recording (SZX16, Olympus) equipped with the DP73 camera (Olympus).

3.5.3 Statistical analysis. All data were presented as the mean $\pm$ standard deviation (SD) from three independent experiments. The statistical significance between each test solution and control was determined by using one-way analysis of variance (ANOVA) followed by Tukey's test to compare the differences between groups. The results were considered statistically differences at a p-value of less than 0.05.

4. Results and discussion

4.1 Physico-chemical characterizations of the composite powders

The FT-IR spectra were used to confirm the chemical functional groups of as-prepared ZAS, CMS and ZASCMS composite powders as shown in Fig. 1. FT-IR spectra of composite materials showed the predominance broad band in the region of
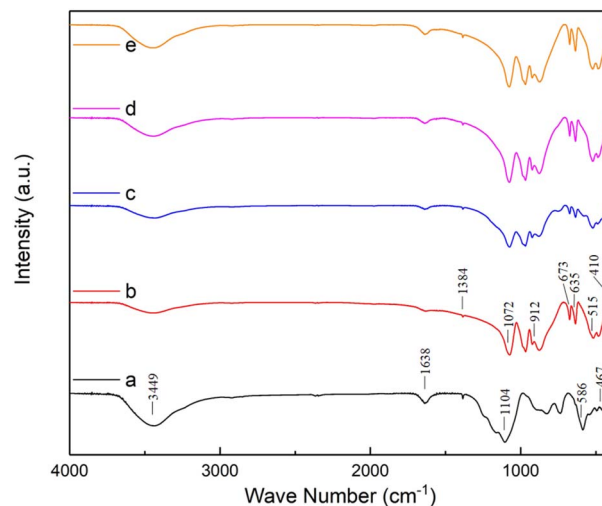

Fig. 1 The FT-IR spectra of ZASCMS composite scaffolds. ZAS (a), CMS (b), ZASCMS25 (c), ZASCMS50 (d) and ZASCMS75 (e) composite scaffolds.

3449 cm^{-1} and a peak at 1638 cm^{-1} due to the absorbed water molecules, which were ascribed to bending and stretching vibrations of O–H bonds. The peak at 1384 cm^{-1} was due to the non-bridging OH group.[33,34] According to the FT-IR spectra of ZAS (Fig. 1(a)), the characteristic peaks at 1104, 1072 and 586 cm^{-1} corresponded to bending vibration of Si–O group,[19] while, the peak at around 875 cm^{-1} indicated the presence of CaO$_3$.[35] Preservation of zirconia in ZAS precursor was confirmed by the spectra at around 467, 586 and 912 cm^{-1} that represented the peaks of Zr–O stretching mode, Zr–O–Zr bending and Zr–OH bending, respectively.[20] The FT-IR spectrum of CMS (Fig. 1(b)) showed the bridging bending vibrating modes of O–Ca–O at 410 cm^{-1} and O–Mg–O at around 515 cm^{-1}. In addition, it showed the doublet at 635 cm^{-1} and 673 cm^{-1}, which was related to the symmetric stretching mode of Si–O–Si.[19,36] As observed in Fig. 1(c–e), the FT-IR spectra of the ZASCMS samples were basically the same absorption peaks, that consisted of the major characteristic spectrums presented by bands of ZAS and CMS phase.

The XRD patterns of ZAS, CMS and ZASCMS composite powders were shown in Fig. 2. The characteristic XRD diffractograms of ZAS powders as shown in Fig. 2(a) showed the crystalline phase of zirconia and alumina silicate that matched with JPCDS data no. 01-089-0889 and 00-002-0415, respectively. These ZAS powders exhibited diffraction peaks with similar pattern to those previously reported,[7] which were attributed to ZrO$_2$ and mullite phases. The diffraction pattern of CMS powder sample (Fig. 2(b)) showed the peak intensities at $2\theta = 26.64°$, 27.58°, 29.84°, 30.26°, 30.87°, 34.93° and 35.53° referring to (021), (220), (2̄21), (310), (3̄11), (1̄31) and (002), respectively, which in turn, corresponded to the formation of diopside with standard cards of JCPDS card no. 00-017-0318. XRD analysis of ZASCMS composite with ZAS to CMS by weight ratios of 3 : 1 (ZASCMS25), 1 : 1 (ZASCMS50) and 1 : 3 (ZASCMS75) as shown in (Fig. 2(c and d)). Although the diffraction pattern of as-
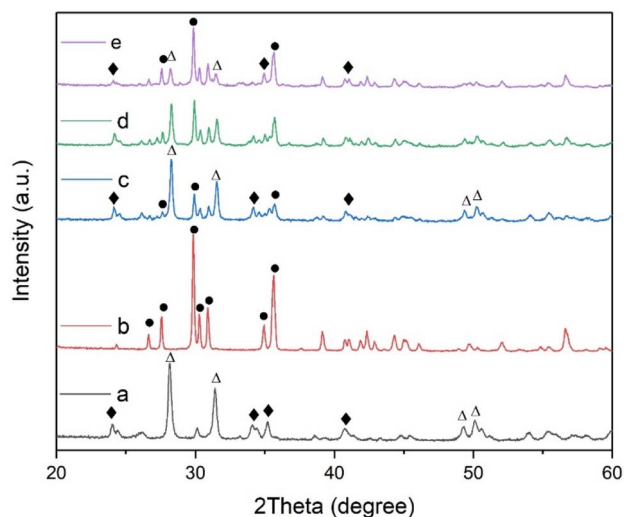
Fig. 2   XRD patterns of synthesized ZASCMS composite scaffolds. ZAS (a), CMS (b), ZASCMS25 (c), ZASCMS50 (d) and ZASCMS75 (e) composite. Δ = ZrO_2 phase, $\blacklozenge$ = mullite phase, $\bullet$ = calcium–magnesium silicate (diopside) phase.

prepared powders showed all three main peaks, zirconia and alumina silicate phase for ZAS and calcium–magnesium-silicate phase for CMS, the XRD patterns were different when compared with the pure substrate. The CMS additive exhibited a relatively low intensity of the ZAS diffraction peaks at $2\theta = 20$–$60°$, especially the peak intensities of ZrO_2 phase appeared to decrease with increasing CMS content. Subsequently, with the CMS content being increased, no new phases were observed in the samples, implying that no reaction occurred between ZAS and CMS particles from the sintering process (the stabilizing the ZAS and CMS phases at 900 °C).

Morphological and elemental analysis of the as-prepared powder of ZAS, CMS and ZASCMS composite powders were elucidated the surface microstructures using SEM as shown in Fig. 3. The pure ZAS powders that were composed of clusters of smaller particles with a size of 300 nm, showed homogeneous porous structure of a few hundred nanometers (Fig. 3(a)). On

the other hand, the morphology of CMS powders (Fig. 3(b)) showed regular crystals and plentiful intergranular micropores with pore sizes in the range of 0.6 to 1.3 μm. The surface microstructures of ZASCMS composites were shown in Fig. 3(c–e). SEM revealed dense microstructure with non-uniform pore size as the amounts of CMS contents in ZAS matrix. The ZASCMS25 (Fig. 3(c)) powder structure was well distributed and appeared more compact than other composite powders. In addition, the SEM image of ZASCMS25 composite powders revealed a relatively uniform distribution of irregular micro-sized particles aggregated in clusters.

As shown in Fig. 3(d), when CMS content reached 50 wt% (ZASCMS50), the distinctive surface morphology of crystalline CMS was observed. The sample became more porous with the increment of CMS, that is, particles, in ZASCMS75 composite (Fig. 3(e)) were apparently more porous with more inter-connected particles in the powders compared to the others. The interconnectivity of ZASCMS apparently occurred with increasing amount of CMS content and contributed to the mechanical strength. Based on the EDS spectra, the element analyses of synthesized ZASCMS50 powders contents repre-sented Zr, Al, Ca, Mg, and Si in the sample (Fig. 3(f)).

Mechanical properties were crucial in the evaluation of suitable scaffolds as implant biomaterials to replace the natural bone. The mechanical properties of the as-prepared ZAS, CMS and ZASCMS composite scaffolds as shown in Fig. 4, showed compressive stress as a function of strain of composites with 2 : 1 height to diameter aspect ratio. Considering the stress–strain curve, in comparison with the pure ZAS the presence of CMS particles appeared to increase the mechanical strength of the ZASCMS scaffold systems, indicating that CMS content had an important influence on the elasticity of the material.

The compressive strength and compressive modulus of the synthesized composite scaffolds were shown in Fig. 5. The compressive strengths of composite scaffolds were 1.92 ± 0.91, 5.25 ± 0.28, 5.70 ± 0.77, 6.78 ± 0.62 and 22.56 ± 1.79 MPa for ZAS, ZASCMS25, ZASCMS50, ZASCMS75 and CMS, respectively
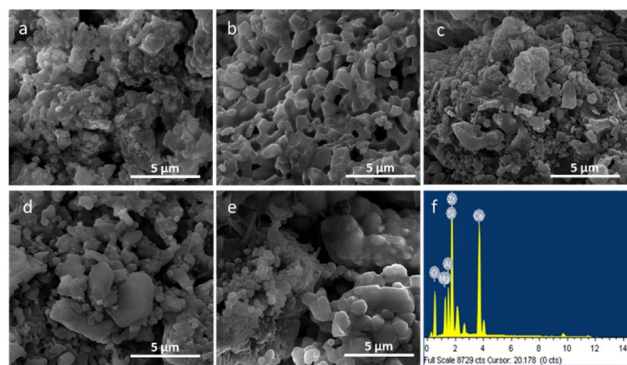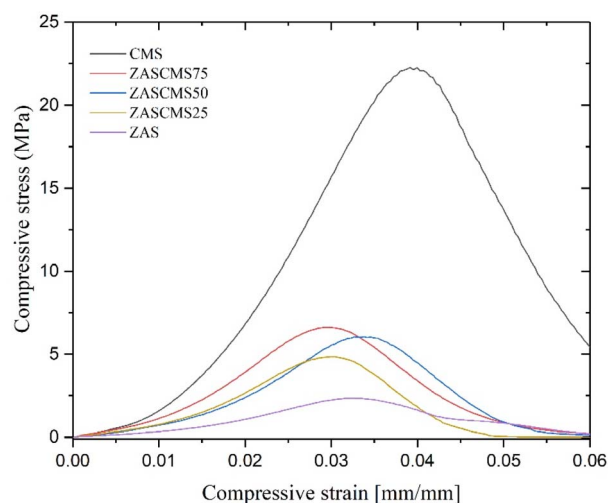

Fig. 3   SEM images of ZASCMS composite scaffolds. ZAS (a), CMS (b), ZASCMS25 (c), ZASCMS50 (d) and ZASCMS75 (e) composite and EDS analysis of ZASCMS50 composite scaffolds (f).

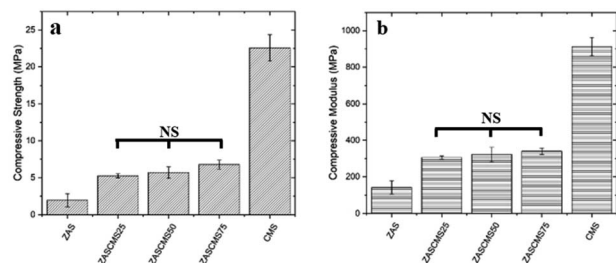Fig. 4   Stress–strain curves of ZAS and CMS contents.

Fig. 5 Compressive strength (a) and compressive modulus (b) of ZAS, CMS and ZASCMS of different ratios. NS is not significant ($p < 0.05$).

(Fig. 5(a)). The strength increased with an increase in CMS content increased, and a similar trend was also found in the compressive modulus as shown in Fig. 5(b). The compressive modulus of ZAS, ZASCMS25, ZASCMS50, ZASCMS75 and CMS composite scaffolds were 141.35 ± 36.53, 305.39 ± 8.97, 321.60 ± 40.43, 340.10 ± 16.81 and 912.18 ± 50.62 MPa, respectively. The gradual increase in compressive strength and modulus of ZASCMS composite scaffolds was possibly contributed by the interconnectivity of calcium-silicate and fewer pores in the matrix, as illustrated in the SEM image (Fig. 3(b)).

4.2 *In vitro* study

The interaction of between cells and the surface of composite scaffold was crucial for cell proliferation, spreading and differentiation.[37] The SEM images of cell adhered on glass (control), ZAS, ZASCMS25, ZASCMS50, ZASCMS75 and CMS scaffold surfaces were shown in Fig. 6(a–f). We investigated cell responses to the scaffold samples after 3 days of incubation. The cells on glass (control) (Fig. 6(a)) showed no differences as compared to those grown on the ZASCMS composite scaffolds. This indicated that the as-prepared scaffold had good biocompatibility and were better for osteoblasts-like UMR-106 cell proliferation. The morphology of UMR-106 cells on ZASCMS50 (Fig. 6(c)) surface exhibited proliferative behaviors, *i.e.*, long spindle cell appearance and smooth cell surface with greater connectivity with neighboring cells, which was a sign of
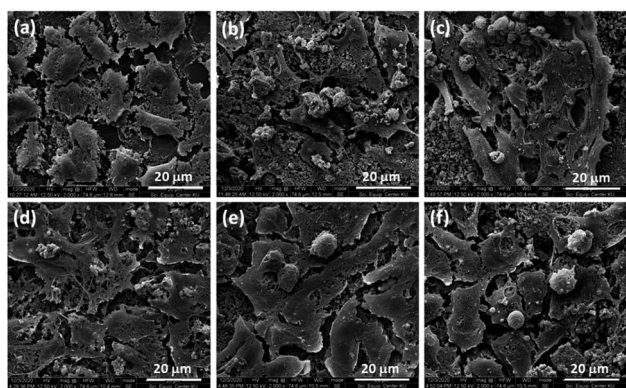

Fig. 6 Representative SEM images of osteoblasts on glass (a) and on ZAS (b), ZASCMS25 (c), ZASCMS50 (d), ZASCMS75 (e) and CMS (f) composite pellet after 3 days of culture.

osteoblastic differentiation. The results of *in vitro* cell behaviors suggested that the amounts of calcium–magnesium-silicate (diopside, CMS) and zirconia–mullite (ZAS) in the scaffolds could affect cell responses to the as-prepared substrate. This phenomenon was probably attributed to the rough surface of composite scaffolds. Previous studies have shown that CMS and zirconia-based composite scaffolds released soluble ionic products (but not investigated in present study) such as Ca, Si and Mg during the *in vitro* degradation test.[13,18] These ionic products were likely to play some roles in enhancing bone cell attachment and proliferation.[7–10]

4.3 Antimicrobial activity of ZASCMS composite scaffolds

The bacteria *S. epidermidis* and *E. coli* were used to investigate the antimicrobial properties of ZAS, CMS, ZASCMS scaffolds. The results were shown in Fig. 7 and Table 1 based on zone inhibition. Our composite materials showed contact inhibition and were able to induce a clear zone as seen in the positive control. The ampicillin diffused from the filter paper to the agar medium surface and inhibited the proliferation of both bacteria, creating a transparent circle around the filter paper as shown in the positive sign region of agar plates. The ZASCMS composite scaffolds were in direct contact with the bacteria, but the ions of composite scaffolds could not diffuse through the solid medium. As a result, there was no proliferation of bacteria only in area around the composite material that was in contact with the medium. Moreover, the image of the ZASCMS composite scaffold surfaces showed that there were no bacteria on the composite material surface, possibly due to the release of Zr^{4+}, Ca^{2+} and Mg^{2+} ions.[38,39] On the other hand, in the negative control group, there was bacterial proliferation under the filter paper. The antibacterial activity of the ZASCMS composite scaffolds was assessed by calculating the percentage of bacterial reduction of *E. coli* and *S. aureus* according to ASTM E2149-13a. Table 1 showed bacteria reduction after 24 h contact time during the incubation of ZASCMS composite scaffolds and inoculum (control). Growth of both bacterial species was inhibited by 99.9%. Our results thus indicated that the composite materials had antibacterial properties. Although the exact mechanism of the antibacterial activity of ZASCMS composite was not fully understood, the physicochemical properties of materials such as charge, roughness, composition are the keys bacteriostatic effects of the materials. In addition, the increased/decreased pH generated by dissolution of ionic species from synthetic material in the test medium can be attributed to inducing an antimicrobial behaviour.[18] In our work, we can postulate that the change in pH observed during the antibacterial study of ZAS, CMS and ZASCMS had a positive inhibitory effect on Gram positive (*S. epidermidis*) and negative (*E. coli*) bacteria. The pH of all scaffolds was found to increase from 6.1 in the initial to 7.1, 7.3 and 7.5 for ZAS, CMS and ZASCMS, respectively. The increasing pH of the test medium resulting disability in the bacterial cells (increasing osmotic pressure) and the residual caused by dissolution of ions such as Ca, Si, Mg, Zr *i.e.* can get the direct contact with the microorganisms damaging the cell walls which ultimately leads to
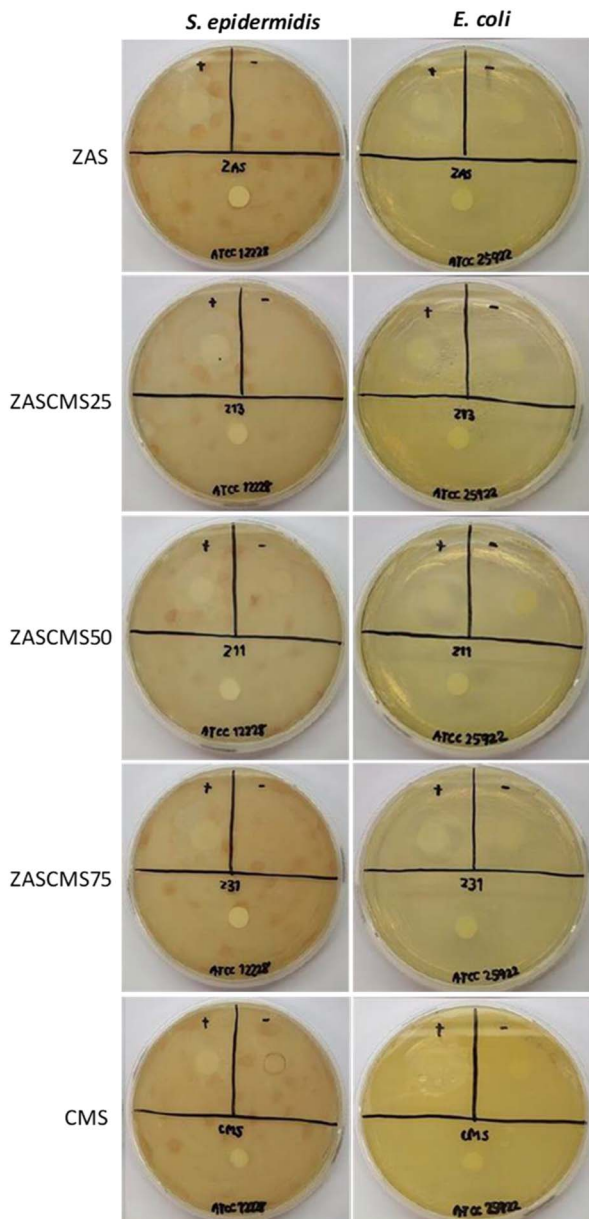
Fig. 7 Antibacterial assay using agar disc-diffusion method against *S. epidermidis* and *E. coli* on ZAS, CMS and ZASCMS composite disc (cylindrical samples with 6 mm diameter and thickness of 2 mm were incubated for 24 h (contact time)).

bacterial death. However, this mechanism still needs to be confirmed by further experiments, (especially for ions release of alkaline ions from ZASCMS composite resulting in an increase

Table 1 The percentage of bacterial reduction after a 24 h incubation

Sample	% reduction of *E. coli*	% reduction of *S. aureus*
ZAS	>99.9	>99.9
ZASCMS25	>99.9	>99.9
ZASCMS50	>99.9	>99.9
ZASCMS75	>99.9	>99.9
CMS	>99.9	>99.9
Inoculum (control)	—	—

in pH, making the surrounding environment unsuitable for bacterial growth), which is the direction of our future research.

4.4 *In vivo* toxicity study of ZASCMS composite scaffolds

Zebrafish has been used as an established vertebrate model for evaluating nanoparticle biocompatibility.[40–44] The fish model has several advantages, such as inexpensive housing, high fecundity rate, rapid development, high genetic homology and high physiological and functional conservation of human genetic make-up.[45,46] As we have known different studies have investigated and reported the effects of calcium phosphate-based bioceramics on embryonic development in zebrafish model. However, the studies were performed with particles at concentration of 0–100 $\mu g\ mL^{-1}$ for hydroxyapatite[40] and at a dose of up to 3000 mg L^{-1} (3000 $\mu g\ mL^{-1}$) for bioactive glass.[41] The present study aimed to evaluate the biocompatibility of the as-prepared particles of ZAS, CMS, and ZASCMS50 by using zebrafish embryos and exposed to the different concentrations of 0–500 $\mu g\ mL^{-1}$. After 96 h exposure of zebrafish embryos to the particles, the survival rates remained unaltered as shown in Fig. 8.

Hatching and heart rates of zebrafish embryos have also been used to evaluate embryotoxicity.[47] In this study, zebrafish in the control group reached 100% hatching rate at 72 hpf, and none of the nanoparticles compromised the hatching rates (Fig. 9). These findings indicated that all the tested nanoparticles did not suppress or delay the developmental process of the zebrafish embryos.

Furthermore, none of the particles altered the heart rates of zebrafish embryos at 24 hpf (Fig. 10). However, at 48 hpf, only CMS significantly reduced the embryonic heart rates at all concentrations tested, as depicted in Fig. 10. Interestingly, other particles with CMS as a component, *e.g.*, ZASCMS50, did not alter the embryonic heart rates (Fig. 10). These results suggested that combining CMS and ZAS could ameliorate the cardiotoxicity of CMS in developing zebrafish embryos.
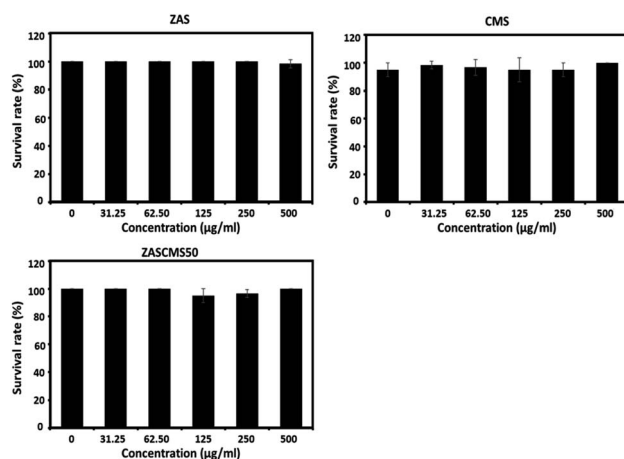

Fig. 8 Survival rates after 96 h exposure of zebrafish embryos exposed to different concentrations of the particles: ZAS, CMS, and ZASCMS50, respectively. The data are from three independent experiments ($n = 3$) and presented as mean ± SD.
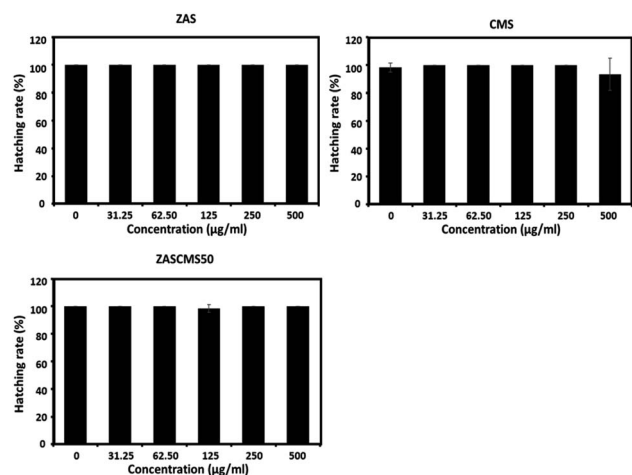
Fig. 9 Hatching rates of zebrafish embryos at 72 hpf after exposure to different concentrations of the particles ZAS, CMS, and ZASCMS50. The data are from three independent experiments ($n = 3$) and presented as mean ± SD.
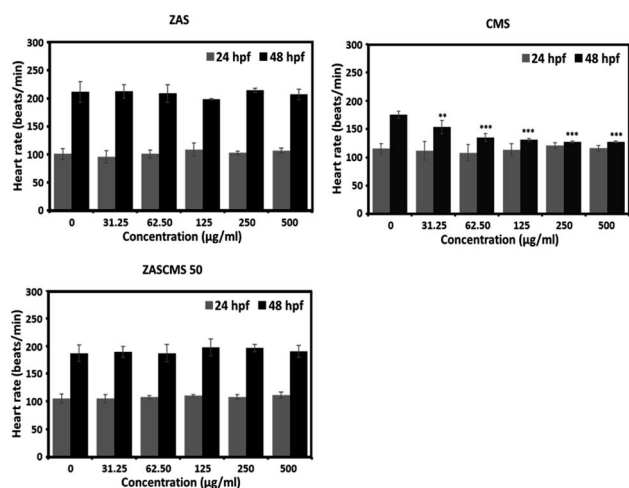

Fig. 10 Heart rates of zebrafish embryos at 24 and 48 hpf after exposure to different concentrations of the particles ZAS, CMS, and ZASCMS50. The data are from three independent experiments ($n = 3$) and presented as mean ± SD. Asterisk represents a statistically significant difference of **$p < 0.01$ and ***$p < 0.001$ versus control.

Fig. 11 Representative images of zebrafish embryos at 72 hpf after exposure to the particles ZAS, CMS, and ZASCMS50. Scale bar = 100 μm.

In the last decade, many bioceramics have been synthesized and developed. However, their toxicological profiles are still limited and certainly require more investigation, especially when they are used as dental materials. There have been a few studies on developmental toxicity studies of dental bioceramics. One biocompatibility study of silver-coated coralline hydroxyapatite in zebrafish embryos[48] demonstrated that after 72 h exposure, there were no effects of the material (1.25 to 3.75 μg mL^{-1}) on embryonic survival, hatching, or heart rates at all exposures. However, the highest concentration caused embryonic abnormalities at 24–72 hpf. In another report, mineral trioxide aggregate and Biodentine were evaluated for their biocompatibility.[49] To evaluate the effects of the particles on
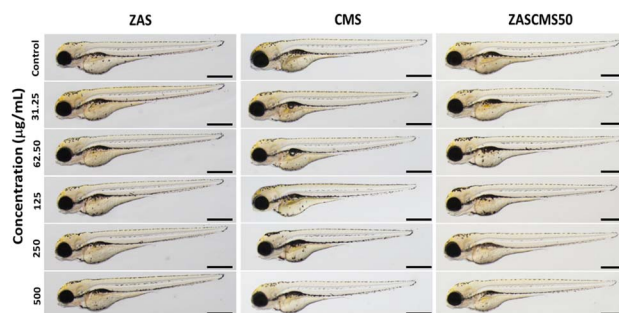
zebrafish morphology, at 72 h exposure after exposure to ZAS, CMS, and ZASCMS50 particles and microscopic images were taken (Fig. 11). Result showed that no malformation of zebrafish embryos/larvae were observed in the treated groups. Therefore, our findings have provided evidence on the developmental toxicity of ZAS and CMS. In addition, we found that ZAS and the mixed particles of ZAS and CMS at the concentrations tested were apparently safe for developing zebrafish. These findings might also imply that ZAS and the composite nanoparticles of ZAS and CMS are biocompatible for humans.

5. Conclusions

In this study, the ZASCMS composite scaffolds were successfully synthesized by the sol–gel technique and investigated for their physiochemical properties, mechanical strength and antimicrobial activity. The ZASCMS50 had suitable contents of ZAS and CMS that enhanced compressive strength and modulus. The surface of ZASCMS composite scaffolds posed no toxicity risk to the rat osteoblast-like UMR-106 cells with good cell adhesion and proliferation. ZASCMS composite scaffolds with more than 50 wt% CMS exhibited a significant increase in mechanical properties and biocompatibility. The in vivo experiment using zebrafish embryos further confirmed that ZASCMS composite particles were not toxic, suggesting that ZASCMS50 (50 wt% of ZAS, 50 wt% of CMS in the scaffold) was a promising candidate for further development as bone tissue applications.

Author contributions

Tanawut Rittidach: methodology, investigation, data analysis and writing-original draft. Siwapech Sillapaprayoon: methodology, investigation. Varissara Chantho: methodology, investigation. Wittaya Pimtong: methodology, investigation, writing-review & editing. Narattaphol Charoenphandhu: conceptualization, formal analysis, data analysis, criticism, conclusion, writing-review & editing, supervision. Jirawan Thongbunchoo: methodology, investigation. Nateetip Krishnamra: writing-review & editing. Atipong Bootchanont: materials synthesis. Porramain Porjai: materials synthesis. Weeraphat Pon-On: conceptualization, formal analysis, resources, funding acquisition, writing-review & editing, supervision.

Conflicts of interest

There are no conflicts to declare.

Acknowledgements

References

1 I. Kovrlija, J. Locs and D. Loca, Octacalcium phosphate: innovative vehicle for the local biologically active substance delivery in bone regeneration, *Acta Biomater.*, 2021, **135**, 27–47.

2 Y. Zhang, T. Shu, S. Wang, Z. Liu, Y. Cheng, A. Li and D. Pei, The osteoinductivity of calcium phosphate-based biomaterials: a tight interaction with bone healing, *Front. Bioeng. Biotechnol.*, 2022, **10**, 911180.

3 S. Samavedi, A. R. Whittington and A. S. Goldstein, Calcium phosphate ceramics in bone tissue engineering: a review of properties and their influence on cell behavior, *Acta Biomater.*, 2013, **9**, 8037–8045.

4 S. E. Lobo and T. L. Arinzeh, Biphasic Calcium Phosphate Ceramics for Bone Regeneration and Tissue Engineering Applications, *Materials*, 2010, **3**, 815–826.

5 J. Jeong, J. H. Kim, J. H. Shim, N. S. Hwang and C. Y. Heo, Bioactive calcium phosphate materials and applications in bone regeneration, *Biomater. Res.*, 2019, **23**, 4.

6 J. R. Jones, Review of Bioactive Glass: From Hench to Hybrids, *Acta Biomater.*, 2013, **9**, 4457–4486.

7 M. N. Rahaman, D. E. Day, B. S. Bal, Q. Fu, S. B. Jung, L. F. Bonewald and A. P. Tomsia, Bioactive glass in tissue engineering, *Acta Biomater.*, 2011, **7**, 2355–2373.

8 S. K. Venkatraman and S. Swamiappan, Review on calcium- and magnesium-based silicates for bone tissue engineering applications, *J. Biomed. Mater. Res., Part A*, 2020, **108**(7), 1546–1562.

9 Y. Huang, X. Jin, X. Zhang, H. Sun, J. Tu, T. Tang, J. Chang and K. Dai, In vitro and in vivo evaluation of akermanite bioceramics for bone regeneration, *Biomaterials*, 2009, **30**, 5041–5048.

10 L. Xia, Z. Yin, L. Mao, X. Wang, J. Liu, X. Jiang, Z. Zhang, K. Lin, J. Chang and B. Fang, Akermanite bioceramics promote osteogenesis, angiogenesis and suppress osteoclastogenesis for osteoporotic bone regeneration, *Sci. Rep.*, 2016, **6**, 22005.

11 M. Kouhia, M. Fathi, V. J. Reddy and S. Ramakrishna, Bredigite Reinforced Electrospun Nanofibers for Bone Tissue Engineering, *Mater. Today: Proc.*, 2019, **7**, 449–454.

12 S. Pang, D. Wu, H. Yang, F. Kamutzki, J. Kurreck, A. Gurlo and D. A. H. Hanaor, Enhanced mechanical performance and bioactivity in strontium/copper co-substituted diopside scaffolds, *Biomater. Adv.*, 2023, **145**, 213230.

13 J. Shen, X. Yang, R. Wu, M. Shen, F. Lu, F. Zhang, Z. Chen, X. Chen, S. Xu, C. Gao and Z. Gou, Direct ink writing core-shell wollastonite@diopside scaffolds with tailorable shell micropores favorable for optimizing physicochemical and biodegradation properties, *J. Eur. Ceram. Soc.*, 2020, **40**, 503–512.

14 P. Ros-Tarraga, P. Mazon, M. A. Sainz, L. Meseguer-Olmo and P. N. De Aza, Surface modifications of a diopside-wollastonite eutectic ceramic after acellular and cellular *in vitro* tests, *Surf. Coat. Technol.*, 2019, **378**, 124965.

15 G. Rathee, G. Bartwal, J. Rathee, Y. K. Mishra, A. Kaushik and P. R. Solanki, Emerging Multimodel Zirconia Nanosystems for High-Performance Biomedical Applications, *Adv. NanoBiomed Res.*, 2021, **1**, 2100039.

16 K. Sakthiabirami, V. Soundharrajan, J. H. Kang, Y. P. Yang and S. W. Park, Three-Dimensional Zirconia-Based Scaffolds for Load-Bearing Bone-Regeneration Applications: Prospects and Challenges, *Materials*, 2021, **14**, 3207.

17 W. Weng, W. Wu, M. Hou, T. Liu, T. Wang and H. Yang, Review of zirconia-based biomimetic scaffolds for bone tissue engineering, *J. Mater. Sci.*, 2021, **56**, 8309–8333.

18 S. J. Ding, Y. H. Chu and P. T. Chen, Mechanical Biocompatibility, Osteogenic Activity, and Antibacterial Efficacy of Calcium Silicate-Zirconia Biocomposites, *ACS Omega*, 2021, **6**, 7106–7118.

19 T. Rittidach, T. Tithito, P. Suntornsaratoon, N. Charoenphandhu, J. Thongbunchoo, N. Krishnamra, I. M. Tang and W. Pon-On, Effect of zirconia-mullite incorporated biphasic calcium phosphate/biopolymer composite scaffolds for bone tissue engineering, *Biomed. Phys. Eng. Express*, 2020, **6**, 055004.

20 K. Sakthiabirami, J. H. Kang, J. G. Jang, V. Soundharrajan, H. P. Lim, K. D. Yun, C. Park, B. N. Lee, Y. P. Yang and S. W. Park, Hybrid porous zirconia scaffolds fabricated using additive manufacturing for bone tissue engineering applications, *Mater. Sci. Eng., C*, 2021, **123**, 111950.

21 A. C. P. Janini, G. F. Bombarda, L. E. Pelepenko and M. A. Marciano, Antimicrobial Activity of Calcium Silicate-Based Dental Materials: A Literature Review, *Antibiotics*, 2021, **10**, 865.

22 P. Muedra, L. Forner, A. Lozano, J. L. Sanz, F. J. Rodríguez-Lozano, J. Guerrero-Gironés, F. Riccitiello, G. Spagnuolo and C. Llena, Could the Calcium Silicate-Based Sealer Presentation Form Influence Dentinal Sealing? An In Vitro

Confocal Laser Study on Tubular Penetration, *Materials*, 2021, **14**, 659.

23 G. T. de Miranda Candeiro, F. C. Correia, M. A. H. Duarte, D. C. Ribeiro-Siqueira and G. Gavini, Evaluation of Radiopacity, pH, Release of Calcium Ions, and Flow of a Bioceramic Root Canal Sealer, *J. Endod.*, 2012, **38**, 842–845.

24 C. Prati and M. G. Gandolfi, Calcium silicate bioactive cements: biological perspectives and clinical applications, *Dent. Mater.*, 2015, **31**, 351–370.

25 Z. Du, H. Leng, L. Guo, Y. Huang, T. Zheng, Z. Zhao, X. Liu, X. Zhang, Q. Cai and X. Yang, Calcium silicate scaffolds promoting bone regeneration via the doping of Mg^{2+} or Mn^{2+} ion, *Composites, Part B*, 2020, **190**, 107937.

26 V. K. Kis, A. Sulyok, M. Hegedus, I. Kovács, N. Rózsa and Z. Kovács, Magnesium incorporation into primary dental enamel and its effect on mechanical properties, *Acta Biomater.*, 2021, **120**, 104–115.

27 C. Coelho, R. Araújo, P. Quadros, S. Sousa and F. Monteiro, Antibacterial bone substitute of hydroxyapatite and magnesium oxide to prevent dental and orthopaedic infections, *Mater. Sci. Eng., C*, 2019, **97**, 529–538.

28 J. E. Lemons, Dental implant biomaterials, *J. Am. Dent. Assoc.*, 1990, **121**, 716–719.

29 W. Pon-On, N. Charoenphandhu, J. Teerapornpuntakit, J. Thongbunchoo, N. Krishnamra and I. M. Tang, Mechanical properties, biological activity and protein controlled release by poly(vinyl alcohol)–bioglass/chitosan–collagen composite scaffolds: a bone tissue engineering applications, *Mater. Sci. Eng., C*, 2014, **38**, 63–72.

30 M. Ahmadipour, H. Mohammadi, A. L. Pang, M. Arjmand, T. A. Otitoju, P. U. Okoye and B. Rajitha, A review: silicate ceramic-polymer composite scaffold for bone tissue engineering, *Int. J. Polym. Mater. Polym. Biomater.*, 2022, **71**, 180–195.

31 American Society for Testing and Materials, *ASTM E2149-13a Standard Test Method for Determining the Antimicrobial Activity of Antimicrobial Agents Under Dynamic Contact Conditions*, 2020, vol. 1, https://www.astm.org/e2149-13a.html.

32 The Organization for Economic Co-operation and Development (OECD), Test No. 236: Fish Embryo Acute Toxicity (FET) Test, *OECD Guidelines for the Testing of Chemicals, Section 2*, OECD Publishing, Paris, 2013, https://www.oecd-ilibrary.org/environment/test-no-236-fish-embryo-acute-toxicity-fet-test_9789264203709-en.

33 S. Mallik, K. M. Parida and S. S. Dash, Studies on heteropoly acid supported zirconia III: oxidative bromination of phenol using phosphotungstic acid supported on zirconia, *J. Mol. Catal. A: Chem.*, 2007, **261**, 172–179.

34 T. N. Rao, I. Hussain, J. E. Lee, A. Kumar and B. H. Koo, Enhanced thermal properties of zirconia nanoparticles and chitosan-based intumescent flame retardant coatings, *Appl. Sci.*, 2019, **9**, 3464.

35 D. Nandhini, S. Subashchandrabose, P. Ramesh, D. M. Radheep and K. Sakthipandi, Synthesis, characterization and computation of potassium doped calcium hydroxide nanoparticle and nanotubes, *International Journal of Mechanical and Production Engineering Research and Development*, 2019, **9**, 441–448.

36 P. Tamilselvi, A. Yelilarasi, M. Hema and R. Anbarasan, Synthesis of hierarchical structured MgO by sol-gel method, *Nano Bull.*, 2013, **2**, 130106.

37 T. Tithito, P. Suntornsaratoon, N. Charoenphandhu, J. Thongbunchoo, N. Krishnamra, I. M. Tang and W. Pon-On, Fabrication of biocomposite scaffolds made with modified hydroxyapatite inclusion of chitosan-grafted-poly(methyl methacrylate) for bone tissue engineering application, *Biomed. Mater.*, 2019, **14**(2), 025013.

38 M. M. Babu, P. S. Prasad, S. H. Bindu, P. V. Rao, N. P. Govindan, N. Veeraiah and M. Özcan, Bioactivity, antibacterial activity and functionality of zirconia doped zinc phosphate bioglasses for application in dentistry, *Mater. Sci. Eng., C*, 2020, **114**, 111052.

39 C. Liu, P. Wan, L. L. Tan, K. Wang and K. Yang, Preclinical investigation of an innovative magnesium-based bone graft substitute for potential orthopaedic applications, *J. Orthop. Transl.*, 2014, **2**, 139–148.

40 S. Pujari-Palmer, X. Lu and M. K. Ott, The Influence of Hydroxyapatite Nanoparticle Morphology on Embryonic Development in a Zebrafish Exposure Model, *Nanomaterials*, 2017, **7**, 89.

41 L. B. Romero-Sánchez, M. Marí-Beffa, P. Carrillo, M. Á. Medina and A. Díaz-Cuenca, Copper-containing mesoporous bioactive glass promotes angiogenesis in an in vivo zebrafish model, *Acta Biomater.*, 2018, **68**, 272–285.

42 M. Ema, K. S. Hougaard, A. Kishimoto and K. Honda, Reproductive and developmental toxicity of carbon-based nanomaterials: a literature review, *Nanotoxicology*, 2016, **10**(4), 391–412.

43 E. Haque and A. C. Ward, Zebrafish as a model to evaluate nanoparticle toxicity, *Nanomaterials*, 2018, **8**(7), 561.

44 L. Chen, J. Li, Z. Chen, Z. Gu, L. Yan, F. Zhao and A. Zhang, Toxicological evaluation of graphene-family nanomaterials, *J. Nanosci. Nanotechnol.*, 2020, **20**(4), 1993–2006.

45 K. Howe, M. D. Clark, C. F. Torroja, J. Torrance, C. Berthelot, M. Muffato, J. E. Collins, S. Humphray, K. McLaren, L. Matthews, S. McLaren, I. Sealy, M. Caccamo, C. Churcher, C. Scott, J. C. Barrett, R. Koch, G. J. Rauch, S. White, W. Chow, B. Kilian, L. T. Quintais, J. A. Guerra-Assunção, Y. Zhou, Y. Gu, J. Yen, J. H. Vogel, T. Eyre, S. Redmond, R. Banerjee, J. Chi, B. Fu, E. Langley, S. F. Maguire, G. K. Laird, D. Lloyd, E. Kenyon, S. Donaldson, H. Sehra, J. Almeida-King, J. Loveland, S. Trevanion, M. Jones, M. Quail, D. Willey, A. Hunt, J. Burton, S. Sims, K. McLay, B. Plumb, J. Davis, C. Clee, K. Oliver, R. Clark, C. Riddle, D. Elliot, G. Threadgold, G. Harden, D. Ware, S. Begum, B. Mortimore, G. Kerry, P. Heath, B. Phillimore, A. Tracey, N. Corby, M. Dunn, C. Johnson, J. Wood, S. Clark, S. Pelan, G. Griffiths, M. Smith, R. Glithero, P. Howden, N. Barker, C. Lloyd, C. Stevens, J. Harley, K. Holt, G. Panagiotidis, J. Lovell, H. Beasley, C. Henderson, D. Gordon, K. Auger, D. Wright, J. Collins, C. Raisen, L. Dyer, K. Leung, L. Robertson, K. Ambridge, D. Leongamornlert, S. McGuire,

R. Gilderthorp, C. Griffiths, D. Manthravadi, S. Nichol, G. Barker, S. Whitehead, M. Kay, J. Brown, C. Murnane, E. Gray, M. Humphries, N. Sycamore, D. Barker, D. Saunders, J. Wallis, A. Babbage, S. Hammond, M. Mashreghi-Mohammadi, L. Barr, S. Martin, P. Wray, A. Ellington, N. Matthews, M. Ellwood, R. Woodmansey, G. Clark, J. Cooper, A. Tromans, D. Grafham, C. Skuce, R. Pandian, R. Andrews, E. Harrison, A. Kimberley, J. Garnett, N. Fosker, R. Hall, P. Garner, D. Kelly, C. Bird, S. Palmer, I. Gehring, A. Berger, C. M. Dooley, Z. Ersan-Ürün, C. Eser, H. Geiger, M. Geisler, L. Karotki, A. Kirn, J. Konantz, M. Konantz, M. Oberländer, S. Rudolph-Geiger, M. Teucke, C. Lanz, G. Raddatz, K. Osoegawa, B. Zhu, A. Rapp, S. Widaa, C. Langford, F. Yang, S. C. Schuster, N. P. Carter, J. Harrow, Z. Ning, J. Herrero, S. M. Searle, A. Enright, R. Geisler, R. H. Plasterk, C. Lee, M. Westerfield, P. J. de Jong, L. I. Zon, J. H. Postlethwait, C. Nüsslein-Volhard, T. J. Hubbard, H. R. Crollius, J. Rogers and D. L. Stemple, The zebrafish reference genome sequence and its relationship to the human genome, *Nature*, 2013, **496**(7446), 498–503.

46 C. H. Hsu, Z. H. Wen, C. S. Lin and C. Chakraborty, The zebrafish model: use in studying cellular mechanisms for a spectrum of clinical disease entities, *Curr. Neurovasc. Res.*, 2007, **4**(2), 111–120.

47 C. Chakraborty, A. R. Sharma, G. Sharma and S. S. Lee, Zebrafish: a complete animal model to enumerate the nanoparticle toxicity, *J. Nanobiotechnol.*, 2016, **14**(1), 65.

48 H. B. Dani, I. D. Ana and B. Retnoaji, Biocompatibility test of ceramic materials in zebrafish development, *AECon*, Purwokerto, Indonesia, 2020, DOI: 10.4108/eai.19-12-2020.2309120.

49 H. Makkar, S. K. Verma, P. K. Panda, E. Jha, B. Das, K. Mukherjee and M. Suar, *In vivo* molecular toxicity profile of dental bioceramics in embryonic zebrafish (*Danio rerio*), *Chem. Res. Toxicol.*, 2018, **31**(9), 914–923.